

# High-Voltage Off-Stoichiometric Vanadium-Based Pyrophosphate $\text{Na}_{6.51}\text{V}_{3.16}(\text{P}_2\text{O}_7)_4$ for Rechargeable Sodium-Ion Batteries

Honglun Wu,<sup>[a]</sup> Tianzhuo Wen,<sup>[a]</sup> Yan Ding,<sup>[b]</sup> Ronghua Huang,<sup>[a]</sup> Yubin Zeng,<sup>[a]</sup> Xiangjun Pu,<sup>\*[b]</sup> and Zhongxue Chen<sup>\*[a]</sup>

The accessibility of high-performance sodium-ion batteries (SIBs) hinges upon cathodes with high voltage and large reversible capacity. Among the contenders, vanadium-based polyanionic compound with strong inductive effect from anionic group and multiple accessible oxidation states of vanadium emerged as a formidable competitor, however, only limited candidates in this field were reported so far. This manuscript delineated the rational synthesis of a novel off-

stoichiometric pyrophosphate  $\text{Na}_{6.51}\text{V}_{3.16}(\text{P}_2\text{O}_7)_4$ . It delivers a specific capacity of  $102 \text{ mAh g}^{-1}$  at the current density of  $20 \text{ mA g}^{-1}$ , as well as a high discharge median voltage of  $3.87 \text{ V}$  vs.  $\text{Na}^+/\text{Na}$ , rendering it a rare sodium-ion storage host with multi-redox couples ( $\text{V}^{5+/4+}/\text{V}^{3+/2+}$ ). The experimental approach to phase adjustment in this article offers guidelines for exploiting of new cathode materials for high-performance SIBs.

## Introduction

The extensive exploitation of clean energy resources (solar and wind) has promoted the rapid development of rechargeable batteries which act as an efficient energy storage technology.<sup>[1]</sup> Lithium-ion battery has attracted the most attention as the advanced battery technology, however, the scarcity of lithium resources forced researchers to turn to cheaper sodium-ion batteries (SIBs).<sup>[2]</sup> Among various sodium-ion storage cathodes for SIBs, polyanionic compounds exhibit the best structural stability, thereby are beneficial for the safety and long cycle life of the batteries.<sup>[3]</sup> Unfortunately, the inherently heavy molecular weight of polyanion groups lowers the reversible capacit and energy density of these cathodes.<sup>[4]</sup> Incorporating multivalent metal ions as the redox center and elevating the operating voltage by tuning the anions have been regarded as promising approaches to enhance the energy density of polyanionic cathode materials.<sup>[5]</sup>

Vanadium exhibits a wide range of oxidation states (from  $\text{V}^{2+}$  to  $\text{V}^{5+}$ ), enabling it to multiple electron redox, making them promising candidates for sodium cathodes.<sup>[6]</sup> In this scenario, tremendous V-based phosphates/pyrophosphates have been

proposed,<sup>[7]</sup> including  $\text{Na}_3\text{V}_2(\text{PO}_4)_3$ ,<sup>[8]</sup>  $\text{Na}_3\text{V}_2(\text{PO}_4)_2\text{F}_3$ ,<sup>[9]</sup>  $\text{NaVOPO}_4$ ,<sup>[10]</sup>  $\text{Na}_7\text{V}_3(\text{P}_2\text{O}_7)_4$ ,<sup>[11]</sup> and the feasibility of two-electron redox couples ( $\text{V}^{4+}/\text{V}^{3+}$  and  $\text{V}^{5+}/\text{V}^{4+}$ ) have been validated.<sup>[12]</sup> Interestingly, the working potential of V-based cathodes could be further adjusted.<sup>[13]</sup> For instance, the  $\text{V}^{4+}/\text{V}^{3+}$  redox couples can be either activated at a lower potential of  $3.4 \text{ V}$  ( $\text{Na}_3\text{V}_2(\text{PO}_4)_3$ ), or at higher potential of  $\sim 4 \text{ V}$  ( $\text{Na}_3\text{V}_2(\text{PO}_4)_2\text{F}_3$ ,  $\text{Na}_7\text{V}_3(\text{P}_2\text{O}_7)_4$ ).<sup>[14]</sup> And for the mixed  $\text{Na}_3\text{V}_4(\text{P}_2\text{O}_7)_4(\text{PO}_4)$  (NVPP) possessing both  $\text{PO}_4$  and  $\text{P}_2\text{O}_7$  groups, a reversible capacity of  $91.4 \text{ mAh g}^{-1}$  (close to its theoretical capacity of  $92.1 \text{ mAh g}^{-1}$ ) and a voltage plateau of  $3.8 \text{ V}$  were achieved.<sup>[15]</sup>

However, despite of its high voltage, the inferior capacity of NVPP hinders the energy density output. Moreover, the rational synthesis of novel member in this ternary  $\text{Na}_2\text{O}-\text{V}_2\text{O}_5-\text{P}_2\text{O}_5$  region has always been hindered due to several factors. Firstly, the synthesis conditions for pure phase materials are stringent. Secondly, materials with non-stoichiometric ratios may also exist as pure phases, such as  $\text{Na}_3\text{V}_2(\text{PO}_4)_2\text{O}_{1.6}\text{F}_{1.4}$ .<sup>[16]</sup> Hence, the reasonable preparation and purification of the material remains a grand challenge.

Herein, based on the experiences for exploration of stoichiometric  $\text{Na}_7\text{V}_4(\text{P}_2\text{O}_7)_4(\text{PO}_4)$ , we achieved the derivation of a new pyrophosphate structure  $\text{Na}_{6.51}\text{V}_{3.16}(\text{P}_2\text{O}_7)_4$  without the easily formed  $\text{Na}_3\text{V}_2(\text{PO}_4)_3$  impurity, by rational adjusting the ratio of V and P sources in the precursors validating the multiple X-ray diffraction (XRD) spectra and Rietveld refinement results. The as-obtained  $\text{Na}_{6.51}\text{V}_{3.16}(\text{P}_2\text{O}_7)_4/\text{C}$  exhibited a specific capacity of  $102 \text{ mAh g}^{-1}$  at the current density of  $20 \text{ mA g}^{-1}$ , and displayed a high discharge median voltage of  $3.87 \text{ V}$ . Through *ex-situ* X-ray photoelectron spectroscopy (XPS) and XRD, we proposed that the sodium storage mechanism of  $\text{Na}_{6.51}\text{V}_{3.16}(\text{P}_2\text{O}_7)_4/\text{C}$  was based on a single phase (solid solution) process involving the multiple redox couples  $\text{V}^{3+}/\text{V}^{2+}$ ,  $\text{V}^{4+}/\text{V}^{3+}$  and  $\text{V}^{5+}/\text{V}^{4+}$ . The experimental approach to achieve phase

[a] H. Wu, T. Wen, Dr. R. Huang, Dr. Y. Zeng, Dr. Z. Chen  
Key Laboratory of Hydraulic Machinery Transients, Ministry of Education,  
School of Power and Mechanical Engineering  
Wuhan University  
Wuhan 430072, China  
E-mail: zxchen\_pmc@whu.edu.cn

[b] Y. Ding, Dr. X. Pu  
College of Chemistry and Molecular Sciences  
Wuhan University  
Wuhan 430072, China  
E-mail: joy\_pu@whu.edu.cn

 Supporting information for this article is available on the WWW under  
<https://doi.org/10.1002/batt.202400076>

purification presented in this study provided insights for phase control and the discovery of more non-stoichiometric materials.

## Results and Discussion

### Rational Derivation of $\text{Na}_{6.51}\text{V}_{3.16}(\text{P}_2\text{O}_7)_4/\text{C}$

In the work of other researchers as well as our preliminary explorations,  $\text{Na}_7\text{V}_4(\text{P}_2\text{O}_7)_4(\text{PO}_4)$  requires sintering at  $800^\circ\text{C}$  to achieve a pure phase. However, when we reduced the sintering temperature to  $650^\circ\text{C}$ , significant changes were observed in the phase characteristics and electrochemical profiles of the material. In specific, Figure S1a presented the XRD spectrum of  $\text{Na}_7\text{V}_4(\text{P}_2\text{O}_7)_4(\text{PO}_4)$  sintered at  $650^\circ\text{C}$ . Nearly all of the NVP peaks could be identified with high intensity, confirming the presence of the  $\text{Na}_3\text{V}_2(\text{PO}_4)_3$  (NVP) phase. Moreover, Figure S1b showed the charge-discharge curves of  $\text{Na}_7\text{V}_4(\text{P}_2\text{O}_7)_4(\text{PO}_4)$  sintered at  $650^\circ\text{C}$ , where it is observable that the curves predominantly consist of two regions, specifically at plateaus around  $3.4\text{ V}$  and approximately  $4\text{ V}$ , with a discharge specific capacity of  $91\text{ mAh g}^{-1}$ . This demonstrated that the reduction in sintering temperature led to the emergence of NVP impurity phases in the material, resulting in a mixed phase of X (unknown phase) and NVP. Due to the formation of NVP, the stoichiometry of phase X deviated from that of  $\text{Na}_7\text{V}_4(\text{P}_2\text{O}_7)_4(\text{PO}_4)$ , and the XRD spectrum and electrochemical characteristics of X (notably the

plateau at approximately  $4\text{ V}$ ) are distinctly different from those of  $\text{Na}_7\text{V}_4(\text{P}_2\text{O}_7)_4(\text{PO}_4)$ . Consequently, X indicated a novel phase.

The purification process of new phase by removing the NVP impurity were then conducted. To eliminate the impurity rationally, primarily assuming the new phase as X, then the composition formula could be expressed by:

$$\text{Na}_7\text{V}_4(\text{P}_2\text{O}_7)_4(\text{PO}_4) = a \cdot [\text{Na}_3\text{V}_2(\text{PO}_4)_3] + b \cdot X$$

Where  $a$  and  $b$  are the constants. Due to the presence of NVP with the Na/V ratio =  $3/2 < 7/4$ , the Na, V stoichiometry in X would larger than  $7/4$ , i.e.,  $\text{Na}/\text{V} > 7/4$ .

To rationally determine its composition, firstly a series of  $\text{Na}_7\text{V}_x\text{P}_9$  ( $x=4, 3.8, 3.6, 3.4$ ) samples were prepared by keeping Na as constant and V as variables. Galvanostatic curves of the sample are presented in Figure 1a. It can be observed that as the V stoichiometry decreasing, the plateau at  $3.4\text{ V}$  becomes significantly narrower and disappears completely in  $\text{Na}_7\text{V}_{3.6}\text{P}_9$  sample, signifying the decrease of NVP impurity, in consistency with the relevant XRD observations in Figure 1b, in which both the complete pattern and enlargements ( $18.5\text{--}21^\circ$  and  $23\text{--}25^\circ$ ) were provided. In the  $18.5\text{--}21^\circ$  range, the characteristic peak of NVP at  $20.06^\circ$  (104) gradually decreased and disappeared. In the  $23\text{--}25^\circ$  range, the characteristic peak of NVP at  $23.76^\circ$  (113) was clearly observed to weaken and disappear. The regular changes in the XRD patterns indicated that during the adjustment of the V ratio, there is a continuous decrease in the

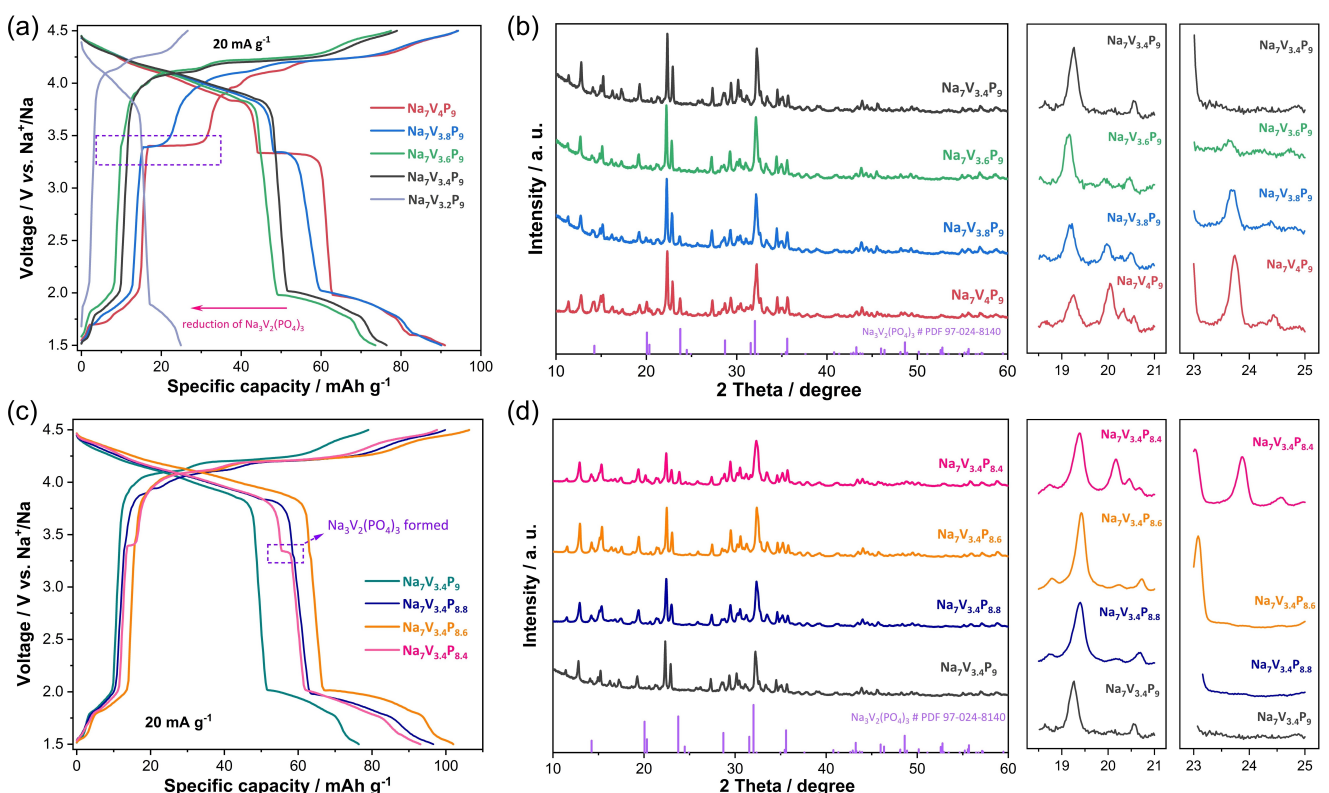


**Figure 1. Derivation of new pyrophosphate structure without the easily formed  $\text{Na}_3\text{V}_2(\text{PO}_4)_3$  impurity.** (a) Charge-discharge profiles of  $\text{Na}_7\text{V}_x\text{P}_9$  samples ( $x=4, 3.8, 3.6, 3.4$ ). (b) X-ray diffraction patterns and enlarged X-ray diffraction patterns of  $\text{Na}_7\text{V}_x\text{P}_9$  samples. (c) Charge-discharge profiles of  $\text{Na}_7\text{V}_{3.4}\text{P}_y$  samples ( $y=9, 8.8, 8.6, 8.4$ ). (d) X-ray diffraction patterns and enlarged patterns of  $\text{Na}_7\text{V}_{3.4}\text{P}_y$  samples.

presence of the NVP phase and an increase in another phase. In addition, as shown in Figure S2, when  $x$  ranges 4 to 3.2 ( $\text{Na}_7\text{V}_{3.2}\text{P}_9$ ), the reversible capacity has dramatically decreased to  $23.4 \text{ mAh g}^{-1}$ .

Moreover, to further polish the performance of primarily determined benchmark sample of  $\text{Na}_7\text{V}_{3.4}\text{P}_9$ , a series of  $\text{Na}_9\text{V}_{3.4}\text{P}_y$  ( $y = 9.5, 9, 8.9, 8.8, 8.7, 8.6, 8.5, 8.4, 8.3$ ) samples were subsequently proposed by keeping V as constant and P as variables. The charge-discharge curves of the  $\text{Na}_9\text{V}_{3.4}\text{P}_y$  ( $y = 9, 8.8, 8.6, 8.4$ ) samples are provided in Figure 1c, and all samples in the extended  $y$  range of  $\text{Na}_7\text{V}_{3.4}\text{P}_y$  were attached in Figure S3. It can be seen that before the P stoichiometry decreases to 8.5, the plateau at 3.4 V did not appear and the reversible capacity shows an increasing trend. When the P stoichiometry continues to decrease from 8.5, the plateau at 3.4 V appeared and gradually widened, indicating the formation of the NVP phase. Similarly,  $\text{Na}_9\text{V}_{3.4}\text{P}_y$  samples were subjected to XRD analysis, with the results presented in the Figure 1d. Within the range of  $18.5^\circ$ – $21^\circ$ , the  $\text{Na}_9\text{V}_{3.4}\text{P}_{8.4}$  sample exhibited diffraction peaks characteristic from NVP, as well as for the range of  $23^\circ$ – $25^\circ$ . This indicated that NVP is regenerated when the P ratio is reduced to 8.4. These results further confirm that the adjustment of the V/P ratio is a purification process of the phase.

Additionally, in order to determine the optimal sintering temperature of  $\text{Na}_7\text{V}_{3.4}\text{P}_{8.6}$ , sintering and testing were conducted in the range of 600–800 °C. Figure S4 and S5 showed the galvanostatic curves and XRD spectra of the samples at different temperatures. It can be observed that the phase structure and electrochemical properties of the material change after exceeding a temperature of 650 °C and the optimal sintering temperature of 650 °C was determined.

### Characterizations of $\text{Na}_{6.51}\text{V}_{3.16}(\text{P}_2\text{O}_7)_4/\text{C}$

Inductively coupled plasma-atomic emission spectroscopy (ICP-AES) was used to confirm the elemental ratios in the sample, and the normalized Na/V/P ratio is 3.24/1.58/4, which is in good agreement with the stoichiometric ratio of the designed chemical formula of  $\text{Na}_{6.51}\text{V}_{3.16}(\text{P}_2\text{O}_7)_4$ . The full XPS spectrum results in Figure S6, confirmed the presence of Na, V, P, O, and C elements. Moreover, Rietveld refinement was performed to confirm the crystal structure of this nonstoichiometric material. As shown in Figure 2a, it turned out that  $\text{Na}_{6.51}\text{V}_{3.16}(\text{P}_2\text{O}_7)_4/\text{C}$  belongs to  $\text{C}2/\text{c}$  space group with unit-cell parameters as  $a = 9.5448 \text{ \AA}$ ,  $b = 8.3643 \text{ \AA}$ ,  $c = 27.6454 \text{ \AA}$ ,  $\beta = 93.622^\circ$ , and the cell volume of  $2202.69 \text{ \AA}^3$ . The relatively low  $R$  values ( $R_p = 6.036\%$ ,  $R_{wp} = 6.694\%$ ) confirm the reliability of the refinement results. Table S1 provided detailed structure information of  $\text{Na}_{6.51}\text{V}_{3.16}(\text{P}_2\text{O}_7)_4$ . Figure 2b showed the schematic crystal structure of  $\text{Na}_{6.51}\text{V}_{3.16}(\text{P}_2\text{O}_7)_4/\text{C}$  based on the refined information from the XRD pattern.

In the framework, the open 3D frameworks built up from corner-sharing  $\text{VO}_6$  octahedra created feasible channels for  $\text{Na}^+$  ions diffusion. SEM and TEM were applied to observe the morphology and microstructure of  $\text{Na}_{6.51}\text{V}_{3.16}(\text{P}_2\text{O}_7)_4/\text{C}$ . Figure 2c and Figure 2d show the SEM images of the sample, which

exhibits spheres ranging from several micrometers to tens of micrometers in size, typical of the spray-drying method. The thickness of the *in-situ* formulated conductive carbon layer is about 4 nm based on the high-resolution TEM (HRTEM) image (Figure 2e). Based on further characterization using Raman spectroscopy in Figure S7, two broadened peaks, namely peak D (at  $1350 \text{ cm}^{-1}$ , indicating  $\text{sp}^3$ -coordinated behavior) and peak G (at  $1590 \text{ cm}^{-1}$ , indicating  $\text{sp}^2$ -coordinated behavior) were detected, and an  $I_D/I_G$  ratio of 1.53 indicated the superior electronic conductivity.<sup>[18]</sup> In addition, the prominent lattice fringes of 0.37 nm corresponding to the (024) plane was observed, indicating the excellent crystallinity. The larger-scale energy dispersive spectroscopy (EDS) measurement in Figure 2f demonstrated the uniform distribution of Na, V and P within the obtained sample.

### Sodium Storage Mechanism

The redox activity of  $\text{Na}_{6.51}\text{V}_{3.16}(\text{P}_2\text{O}_7)_4/\text{C}$  was investigated by *ex-situ* XPS spectra for V 2p (Figure 3a) at the pristine, fully desodiated and sodiated states. In the pristine state, the V 2p<sub>3/2</sub> and V 2p<sub>1/2</sub> peaks corresponding to  $\text{V}^{3+}$  are evident at 516.5 and 523.9 eV, respectively, in consistency with the formula composition.<sup>[19]</sup> After charging to 4.5 V, the V 2p<sub>3/2</sub> and V 2p<sub>1/2</sub> peaks shift to higher energy and can be divided into two pairs. The peaks at 517.3 and 524.6 eV correspond to  $\text{V}^{4+}$  2p<sub>3/2</sub> and  $\text{V}^{4+}$  2p<sub>1/2</sub>, while the peaks at 518.2 and 525.5 eV correspond to  $\text{V}^{5+}$  2p<sub>3/2</sub> and  $\text{V}^{5+}$  2p<sub>1/2</sub>.<sup>[20]</sup> The peak of V 2p returns to a lower state, indicated as  $\text{V}^{3+}$  and  $\text{V}^{2+}$  ( $\text{V}^{2+}$  2p<sub>3/2</sub> located at 515.3 and  $\text{V}^{2+}$  2p<sub>1/2</sub> located at 522.8 eV), when discharged to 1.5 V. This demonstrated two key points that the electrode exhibited good reversibility and it operated through multiple redox couples including  $\text{V}^{3+}/\text{V}^{2+}$ ,  $\text{V}^{4+}/\text{V}^{3+}$  and  $\text{V}^{5+}/\text{V}^{4+}$  during sodium extraction and insertion. Note that a similar conclusion was confirmed in the stoichiometric pyrophosphate  $\text{Na}_7\text{V}_3(\text{P}_2\text{O}_7)_4$ , wherein the activation of  $\text{V}^{3+}/\text{V}^{2+}$  and  $\text{V}^{5+}/\text{V}^{4+}$  redox couple occurred during charging and discharging within a wide voltage window of 1.35–4.8 V.<sup>[12a]</sup>

In addition, *ex-situ* XRD measurements were conducted on electrodes at different state of charge (SoC) to study the structure changes. Figure 3b illustrated the XRD patterns of the pristine sample, samples charged to 3.8 V, 4.3 V, and 4.5 V, as well as samples discharged to 3.7 V and 1.5 V. In the XRD patterns, all major diffraction peaks (except for the peak at  $22.19^\circ$  (022) and peak at  $22.78^\circ$  (130)) underwent a slight right shift during charging, indicating a decrease in interplanar spacing, and reversibly return to their original positions, demonstrating the reversibility of the charge/discharge process. Meanwhile, no disappearance of diffraction peaks or appearance of new diffraction peaks were observed, suggesting a single phase (solid solution) process manner. Based on the information from *ex-situ* XRD, calculations were further performed on the lattice changes during the charge-discharge process. During charging, the lattice parameter  $a$  increased from  $9.544 \text{ \AA}$  to  $9.593 \text{ \AA}$ , the lattice parameter  $c$  increased from  $27.645 \text{ \AA}$  to  $27.726 \text{ \AA}$ , and the lattice parameter  $b$  decreased

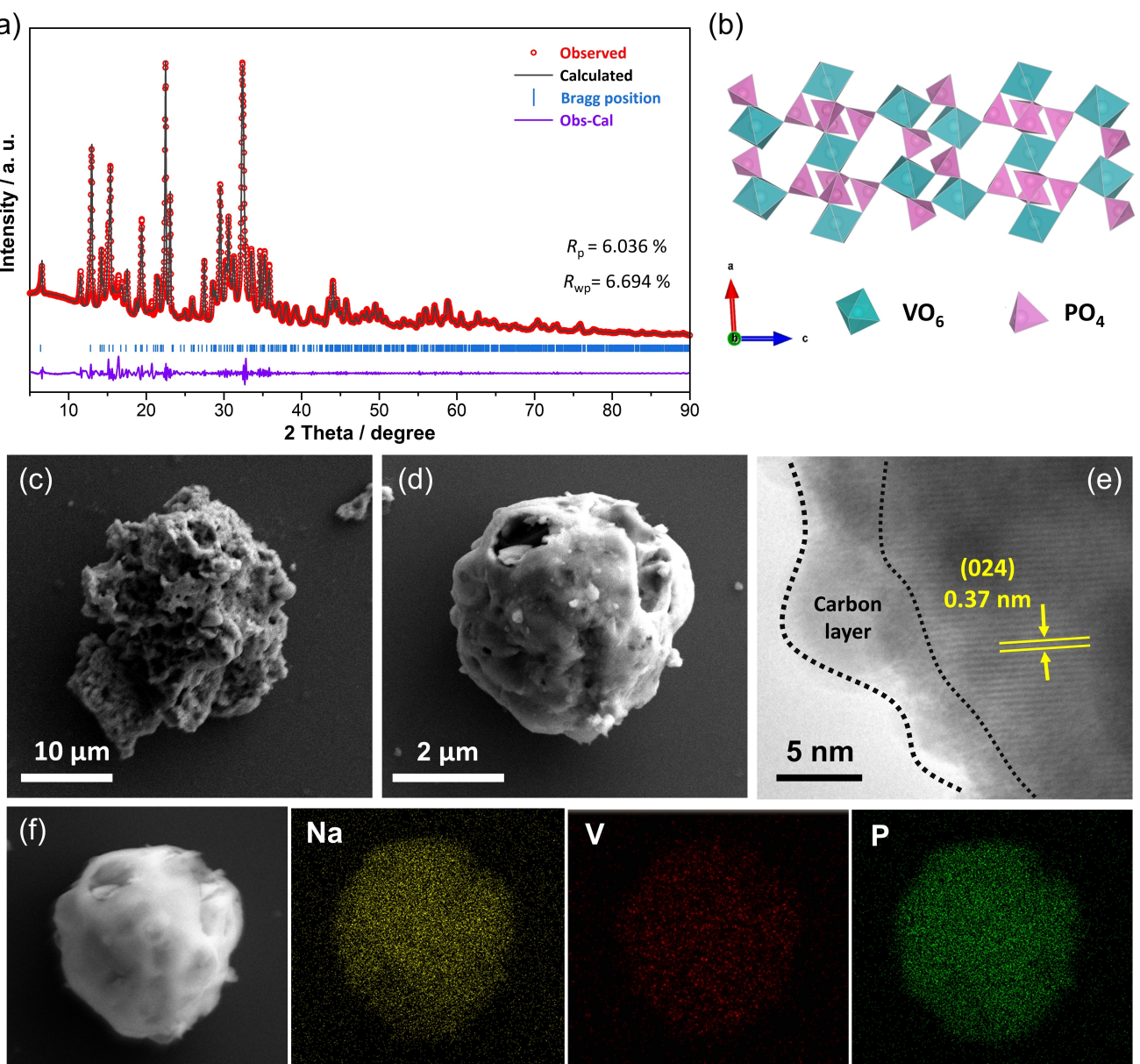


**Figure 2. Characterizations of  $\text{Na}_{6.51}\text{V}_{3.16}(\text{P}_2\text{O}_7)_4/\text{C}$  sample.** (a) Rietveld refinement of  $\text{Na}_{6.51}\text{V}_{3.16}(\text{P}_2\text{O}_7)_4$ . (b) Schematic polyanionic framework of  $\text{Na}_{6.51}\text{V}_{3.16}(\text{P}_2\text{O}_7)_4$ . (c) and (d) Scanning electron microscopy (SEM) images with different resolutions. (e) The high-resolution transmission electron microscopy (HRTEM) image of  $\text{Na}_{6.51}\text{V}_{3.16}(\text{P}_2\text{O}_7)_4/\text{C}$ . (f) SEM-EDS mapping of  $\text{Na}_{6.51}\text{V}_{3.16}(\text{P}_2\text{O}_7)_4/\text{C}$ .

from 8.364 Å to 8.021 Å, with an overall change in cell volume of approximately 4%.

#### Electrochemical Performance of $\text{Na}_{6.51}\text{V}_{3.16}(\text{P}_2\text{O}_7)_4/\text{C}$

The charge-discharge curves of the sample for the first three cycles are shown in Figure 4a. At a current density of 20 mA g<sup>-1</sup>, the electrode delivered a reversible capacity of 102 mAh g<sup>-1</sup>. The CV curves of  $\text{Na}_{6.51}\text{V}_{3.16}(\text{P}_2\text{O}_7)_4/\text{C}$  in the voltage window of 1.5–4.5 V with a scan rate of 0.1 mV s<sup>-1</sup> was shown in Figure 4b. The sample exhibits four pairs of oxidation/reduction peaks at 4.45/4.35 V, 4.3/4.1 V, 4.15/3.88 V, and 1.88/1.86 V, corresponding to the extraction and insertion of sodium ions. CV measure-

ments and galvanostatic cycling revealed quite unusual electrochemical behavior of  $\text{Na}_{6.51}\text{V}_{3.16}(\text{P}_2\text{O}_7)_4/\text{C}$ : during the initial charging process within the voltage range of 2.3–4.5 V, a specific capacity of 95.7 mAh g<sup>-1</sup> was released, corresponding to the intercalation of 1.8 Na<sup>+</sup> ions. The theoretical capacity for the " $\text{Na}_{6.51}\text{V}_{3.16}^{+3}(\text{P}_2\text{O}_7)_2 \leftrightarrow \text{Na}_{6.51}\text{V}_{3.16}^{+4}(\text{P}_2\text{O}_7)_2$ " is 84.1 mAh g<sup>-1</sup>, and additional capacity can be attributed to the activation of V<sup>4+</sup>/V<sup>5+</sup> reaction, as validated by above mechanisms discussion.

It is noteworthy that a significant asymmetry between deintercalation and intercalation processes is recognized, which is originated mainly from multiple sodium sites with unequal energies or for various cations possessing distinct redox potentials, and similar voltage asymmetry were observed in the typical V-based counterparts like  $\text{Na}_3\text{V}_2(\text{PO}_4)_2\text{F}_3$ ,<sup>[21]</sup>  $\beta\text{-NaVP}_2\text{O}_7$ ,<sup>[22]</sup>

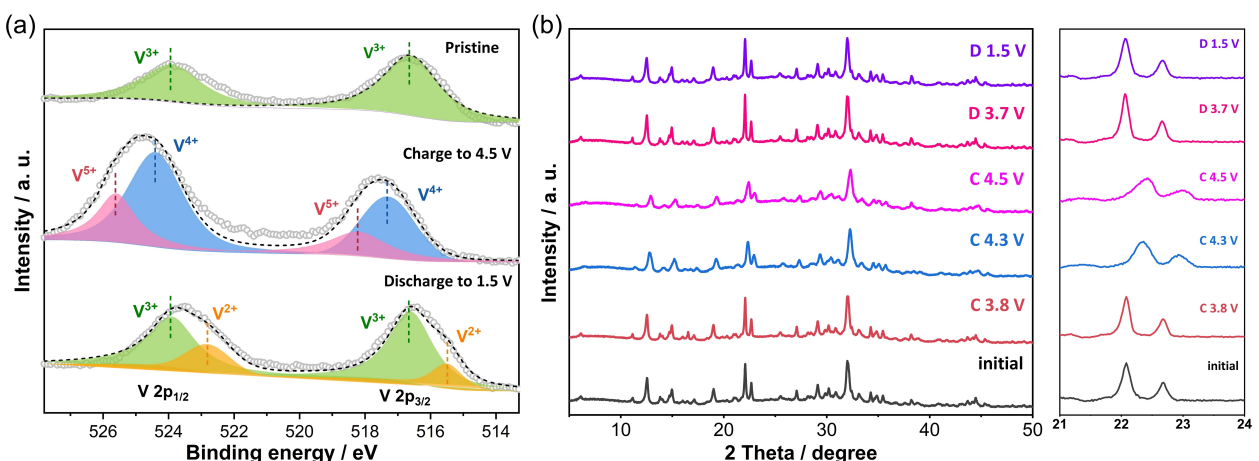


**Figure 3.** Ex-situ spectrum analysis for reaction mechanisms. (a) XPS spectra of V 2p at different states. (b) XRD patterns of  $\text{Na}_{6.51}\text{V}_{3.16}(\text{P}_2\text{O}_7)_4/\text{C}$  samples at different charge-discharge states and the enlarged XRD patterns from  $21^\circ$  to  $24^\circ$ .

and  $\text{Na}_7\text{V}_3(\text{P}_2\text{O}_7)_4$ .<sup>[12a]</sup> Furthermore, the material retained a reversible capacity of  $67.8 \text{ mAh g}^{-1}$ , which was 70.1% of its initial capacity after 150 cycles at  $20 \text{ mA g}^{-1}$  in the voltage window of  $1.5$ – $4.5 \text{ V}$  (Figure 4c). The electrode also exhibited decent cycling stability within narrowed window of  $2.5$ – $4.2 \text{ V}$  (Figure S8), but certainly with decreased capacity. The rate performances presented in Figure 4d were carried out under varying current densities ranging from  $20$  to  $2000 \text{ mA g}^{-1}$ , and the electrodes demonstrated reversible capacities of  $97.5$ ,  $86.5$ ,  $82.9$ ,  $75.8$ ,  $58.2$ , and  $43.7 \text{ mAh g}^{-1}$  against the ramped current densities. A reversible capacity of  $99.2 \text{ mAh g}^{-1}$  could be harvested when the current recovered to  $20 \text{ mA g}^{-1}$ , indicating the stability of the polyanionic structure to withstand high currents. The dynamic performance of  $\text{Na}_{6.51}\text{V}_{3.16}(\text{P}_2\text{O}_7)_4/\text{C}$  was further estimated by galvanostatic intermittent titration technique (GITT). A constant current flux of  $0.1 \text{ C}$  was applied to the electrodes for  $10$  minutes to control sodium storage, followed by a relaxation process for  $30$  minutes. The calculation of  $D_{\text{Na}^+}$  is based on the equation below:

$$D_{\text{Na}^+} = \frac{4}{\pi\tau} \left( \frac{m_B V_m}{M_B S} \right)^2 \frac{4}{\pi\tau} \left( \frac{\Delta E_s}{\Delta E_t} \right)^2 \quad \tau \ll \frac{l^2}{D_{\text{Na}^+}}$$

where  $m_B$ ,  $M_B$ ,  $V_m$ ,  $S$  represent mass, molecular weight, molar volume and surface area of the cathode material respectively.  $\Delta E_s$  is the difference between two consecutive stable voltages after relaxation, and  $\Delta E_t$  is the transient voltage-change during a single titration step. The GITT profiles of the electrode were shown in Figure 4e, and the relevant diffusion coefficients were further calculated in the order of  $10^{-12} \text{ cm}^2 \text{s}^{-1}$  (in Figure 4e), comparable to that of NASICON-type materials, indicating good dynamic performance of the cathode material.<sup>[23]</sup>

## Conclusions

In this work, we have achieved rational derivation of novel pyrophosphate structure based on the exploration of the

synthesis of  $\text{Na}_7\text{V}_4(\text{P}_2\text{O}_7)_4(\text{PO}_4)$ , by adjusting the ratio of V and P sources in the raw materials. The new pyrophosphate was identified as  $\text{Na}_{6.51}\text{V}_{3.16}(\text{P}_2\text{O}_7)_4/\text{C}$ , which exhibited a reversible capacity of  $102 \text{ mAh g}^{-1}$  at a current density of  $20 \text{ mA g}^{-1}$  and a high discharge median voltage of  $3.87 \text{ V}$ . A single phase (solid solution) process was revealed together with the activation of blended  $\text{V}^{3+}/\text{V}^{2+}$ ,  $\text{V}^{4+}/\text{V}^{3+}$  and  $\text{V}^{5+}/\text{V}^{4+}$  redox couples. The methodology of phase purification demonstrated in this contribution offers strategic guidance for identifying hidden high-voltage non-stoichiometric cathode materials for sodium-ion batteries.

## Experimental Section

### Material Preparation

The  $\text{Na}_{6.51}\text{V}_{3.16}(\text{P}_2\text{O}_7)_4$  sample was synthesized by a simple spray-dried method with a subsequent high temperature annealing. Firstly,  $21 \text{ mmol}$   $\text{NaH}_2\text{PO}_4 \cdot 2\text{H}_2\text{O}$ ,  $4.8 \text{ mmol}$   $\text{NH}_4\text{H}_2\text{PO}_4$ ,  $6 \text{ mmol}$   $\text{C}_6\text{H}_8\text{O}_7 \cdot \text{H}_2\text{O}$ , and  $5.1 \text{ mmol}$   $\text{V}_2\text{O}_5$  were dissolved in  $100 \text{ mL}$  distilled water under continuous stirring at room temperature to get aqua solution. After then, the above solution was spray-dried at  $105^\circ\text{C}$  to get precursor. Finally, the as-prepared sample was annealed at  $650^\circ\text{C}$  for  $12 \text{ h}$  under an Ar atmosphere with a heating rate of  $3^\circ\text{C}$  to form carbon decorated  $\text{Na}_{6.51}\text{V}_{3.16}(\text{P}_2\text{O}_7)_4$  (denoted  $\text{Na}_{6.51}\text{V}_{3.16}(\text{P}_2\text{O}_7)_4/\text{C}$ ). The samples with other Na/V/P ratios were prepared in the same procedures by just adjusting the relevant elementary ratios.

### Characterizations

The spray-drying process was conducted on a spray-drying machine (H-Spray Mini, China). XRD measurements were performed on a Bruker AXS diffractometer (D8 Advance) with a monochromated Cu K $\alpha$  X-ray source. The morphologies and structure were examined by scanning electron microscopy (SEM, ZEISS Merlin Compact, Germany) and transmission electron microscopy (TEM, JEM-2100FEF, Japan). The measurement of Na/V/P stoichiometry was conducted on inductively coupled plasma-atomic emission spectrometry (ICP-AES, IRIS Intrepid II XSP, USA). X-ray photoelectron spectroscopy

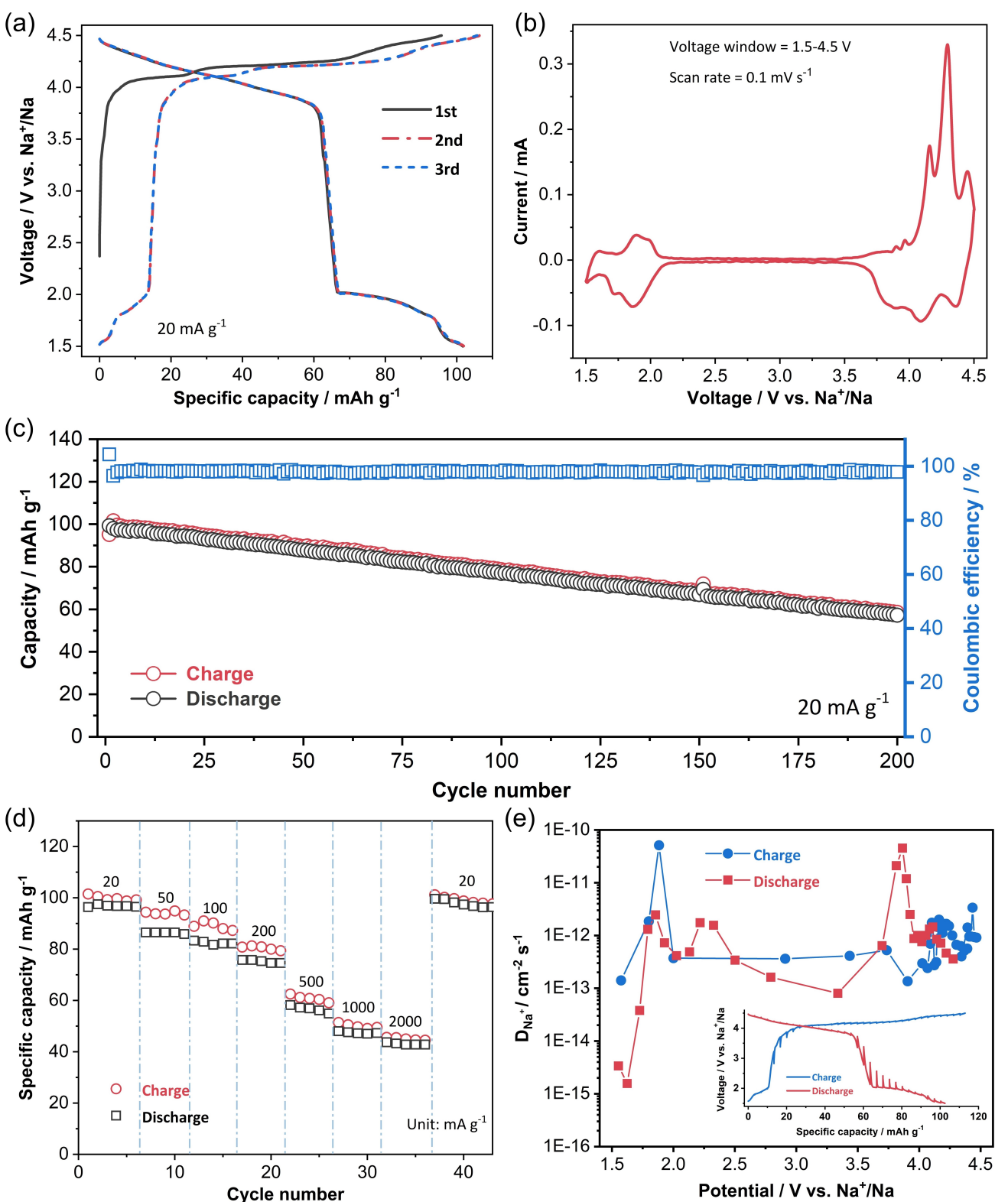


**Figure 4.** Electrochemical performances of  $\text{Na}_{0.651}\text{V}_{3.16}(\text{P}_2\text{O}_7)_4/\text{C}$  samples. (a) The charge-discharge profiles of first three cycles of  $\text{Na}_{0.651}\text{V}_{3.16}(\text{P}_2\text{O}_7)_4/\text{C}$ . (b) The cyclic voltammetry (CV) profiles of  $\text{Na}_{0.651}\text{V}_{3.16}(\text{P}_2\text{O}_7)_4/\text{C}$  in 1.5–4.5 V at  $0.1 \text{ mV s}^{-1}$ . (c) Cycle performance. (d) Rate performance. (e) GITT profiles of  $\text{Na}_{0.651}\text{V}_{3.16}(\text{P}_2\text{O}_7)_4/\text{C}$  and the calculated  $\text{Na}^+$  diffusion coefficient.

(XPS) analysis was carried out on a spectrometer (ESCALAB 250Xi spectrometer, England). The Raman spectroscopic data were

obtained on a Raman microscope (DXR2, Thermo Fisher, America).

## Electrochemical Measurements

The working electrodes were prepared by mixing 80% (mass fraction, as follows) active material, 10% Super P and 10% binder (polyvinylidene difluoride (PVDF) dissolved in N-methyl-2-pyrrolidone (NMP) to form homogeneous slurry. Later, the slurry was pasted on Al foil and dried at 80 °C for 10 h in a vacuum oven. The electrode loading was about 2 mg cm<sup>-2</sup>, and the electrode area was 1.44 cm<sup>2</sup>. The coin cells (CR2032) were assembled in an argon filled glove box with 1 mol L<sup>-1</sup> NaClO<sub>4</sub> dissolved ethylene carbonate/diethyl carbonate (EC/DEC, 1:1 by vol.) with 5% fluoroethylene carbonate (FEC) as the electrolyte, Na foil as reference and counter electrode and a polypropylene microporous film (Celgard 2300) as the separator. The galvanostatic charge/discharge and galvanostatic intermittent titration technique (GITT) measurements were conducted on a LAND CT-2001 test system. Cyclic voltammetric measurements were also conducted with the coin cell on a CHI 660E electrochemical workstation.

## Supporting Information

The authors have cited additional references within the Supporting Information.

## Acknowledgements

This work was financially supported by the National Natural Science Foundation of China (U22A20438, U22A20193), the Key R&D Plan of Hubei Province (2023BAB036), and the Fundamental Research Funds for the Central Universities.

## Conflict of Interests

The authors declare no conflict of interest.

## Data Availability Statement

The data that support the findings of this study are available from the corresponding author upon reasonable request.

**Keywords:** Sodium-ion batteries • High-voltage cathode material • Vanadium-based pyrophosphate • Off-stoichiometric

- [1] D. Zhao, C. Wang, Y. Ding, M. Ding, Y. Cao, Z. Chen, *ChemSusChem* 2022, 15, e202200479.

- [2] X. Pu, H. Wang, D. Zhao, H. Yang, X. Ai, S. Cao, Z. Chen, Y. Cao, *Small* 2019, 25, 1805427.
- [3] a) X. Pu, H. Wang, T. Yuan, S. Cao, S. Liu, L. Xu, H. Yang, X. Ai, Z. Chen, Y. Cao, *Energy Storage Mater.* 2019, 22, 330–336; b) T. Yuan, Y. Wang, J. Zhang, X. Pu, X. Ai, Z. Chen, H. Yang, Y. Cao, *Nano Energy* 2019, 56, 160–168.
- [4] a) H. Wu, Y. Chen, T. Wen, L. Chen, X. Pu, Z. Chen, *Batteries* 2023, 9, 56; b) Y. Fang, Z. Chen, L. Xiao, X. Ai, Y. Cao, H. Yang, *Small* 2018, 14, 1703116; c) Y. Fang, L. Xiao, Z. Chen, X. Ai, Y. Cao, H. Yang, *Electrochim. Energy Rev.* 2018, 1, 294–323.
- [5] Y. You, A. Manthiram, *Adv. Energy Mater.* 2017, 8, 1701785.
- [6] C. Xu, J. Zhao, Y. A. Wang, W. Hua, Q. fu, X. Liang, X. Rong, Q. Zhang, X. Guo, C. Yang, H. Liu, B. Zhong, Y. S. Hu, *Adv. Energy Mater.* 2022, 12, 2200966.
- [7] Z. Lv, M. Ling, M. Yue, X. Li, M. Song, Q. Zheng, H. Zhang, *J. Energy Chem.* 2021, 55, 361–390.
- [8] K. Saravanan, C. W. Mason, A. Rudola, K. H. Wong, P. Balaya, *Adv. Energy Mater.* 2013, 3(4), 444–450.
- [9] a) K. Chihara, A. Kitajou, I. D. Gocheva, S. Okada, J.-i. Yamaki, *J. Power Sources* 2013, 227, 80–85; b) Z. Liu, Y.-Y. Hu, M. T. Dunstan, H. Huo, X. Hao, H. Zou, G. Zhong, Y. Yang, C. P. Grey, *Chem. Mater.* 2014, 26, 2513–2521.
- [10] Y. Fang, Q. Liu, L. Xiao, Y. Rong, Y. Liu, Z. Chen, X. Ai, Y. Cao, H. Yang, J. Xie, C. Sun, X. Zhang, B. Aoun, X. Xing, X. Xiao, Y. Ren, *Chem* 2018, 4, 1–14.
- [11] a) C. Deng, S. Zhang, *ACS Appl. Mater. Interfaces* 2014, 6, 9111–9117; b) S. Zhang, C. Deng, Y. Meng, *J. Mater. Chem. A* 2014, 2, 20538–20544.
- [12] a) V. M. Kovrugin, J.-N. Chotard, F. Fauth, C. Masquelier, *J. Mater. Chem. A* 2020, 8, 21110–21121; b) S.-C. Yin, H. Grondey, P. Strobel, M. Anne, L. F. Nazar, *J. Am. Chem. Soc.* 2003, 125, 10402–10411; c) J. Liu, L. Yin, X.-Q. Yang, P. G. Khalifah, *Chem. Mater.* 2018, 30, 4609–4616.
- [13] M. Chen, Q. Liu, Z. Hu, Y. Zhang, G. Xing, Y. Tang, S. L. Chou, *Adv. Energy Mater.* 2020, 10, 2002244.
- [14] a) L. Deng, F.-D. Yu, Y. Xia, Y.-S. Jiang, X.-L. Sui, L. Zhao, X.-H. Meng, L.-F. Que, Z.-B. Wang, *Nano Energy* 2021, 82, 105659; b) J. Kim, I. Park, H. Kim, K.-Y. Park, Y.-U. Park, K. Kang, *Adv. Energy Mater.* 2016, 6, 1502147; c) Q. Li, B. Lin, S. Zhang, C. Deng, *J. Mater. Chem. A* 2016, 4, 5719–5729.
- [15] V. M. Kovrugin, J.-N. Chotard, F. Fauth, A. Jamali, R. David, C. Masquelier, *J. Mater. Chem. A* 2017, 5, 14365–14376.
- [16] Y. U. Park, D. H. Seo, H. S. Kwon, B. Kim, J. Kim, H. Kim, I. Kim, H. I. Yoo, K. Kang, *J. Am. Chem. Soc.* 2013, 135, 13870.
- [17] Q. Zheng, H. Yi, X. Li, H. Zhang, *J. Energy Chem.* 2018, 27, 1597–1617.
- [18] A. Zhao, T. Yuan, P. Li, C. Liu, H. Cong, X. Pu, Z. Chen, X. Ai, H. Yang, Y. Cao, *Nano Energy* 2022, 91, 106680.
- [19] L. Tang, J. Zhang, Z. Li, X. Liu, Q. Xu, H. Liu, Y. Wang, Y. Xia, Z. Ma, *J. Power Sources* 2020, 451, 227734.
- [20] H. Li, C. Guan, M. Xu, J. Guo, K. Yuan, K. Cheng, Y. Xie, L. Zhang, J. Zheng, Y. Lai, Z. Zhang, *Energy Storage Mater.* 2022, 47, 526–533.
- [21] G. Yan, S. Mariyappan, G. Rousse, Q. Jacquet, M. Deschamps, R. David, B. Mirvax, J. W. Freeland, J. M. Tarascon, *Nat. Commun.* 2019, 10, 585.
- [22] O. A. Drozhzhin, I. V. Tertov, A. M. Alekseeva, D. A. Aksyonov, K. J. Stevenson, A. M. Abakumov, E. V. Antipov, *Chem. Mater.* 2019, 31, 7463–7469.
- [23] Z. Yang, G. Li, J. Sun, L. Xie, Y. Jiang, Y. Huang, S. Chen, *Energy Storage Mater.* 2020, 25, 724–730.

Manuscript received: February 2, 2024  
Revised manuscript received: April 7, 2024  
Accepted manuscript online: April 8, 2024  
Version of record online: May 2, 2024